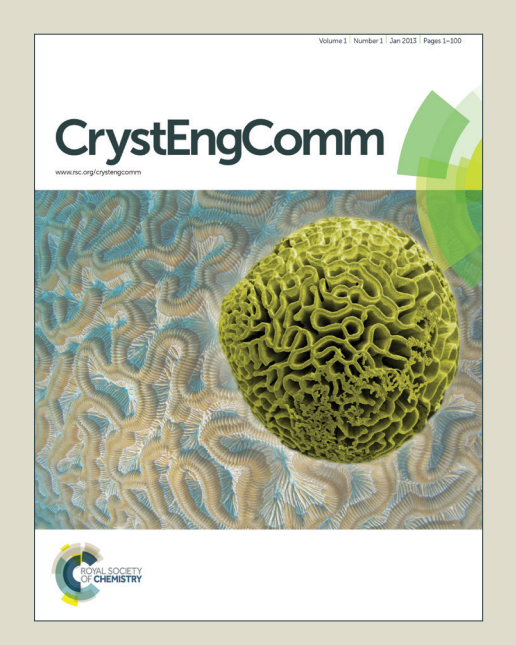
CrystEngComm

Accepted Manuscript



This is an *Accepted Manuscript*, which has been through the Royal Society of Chemistry peer review process and has been accepted for publication.

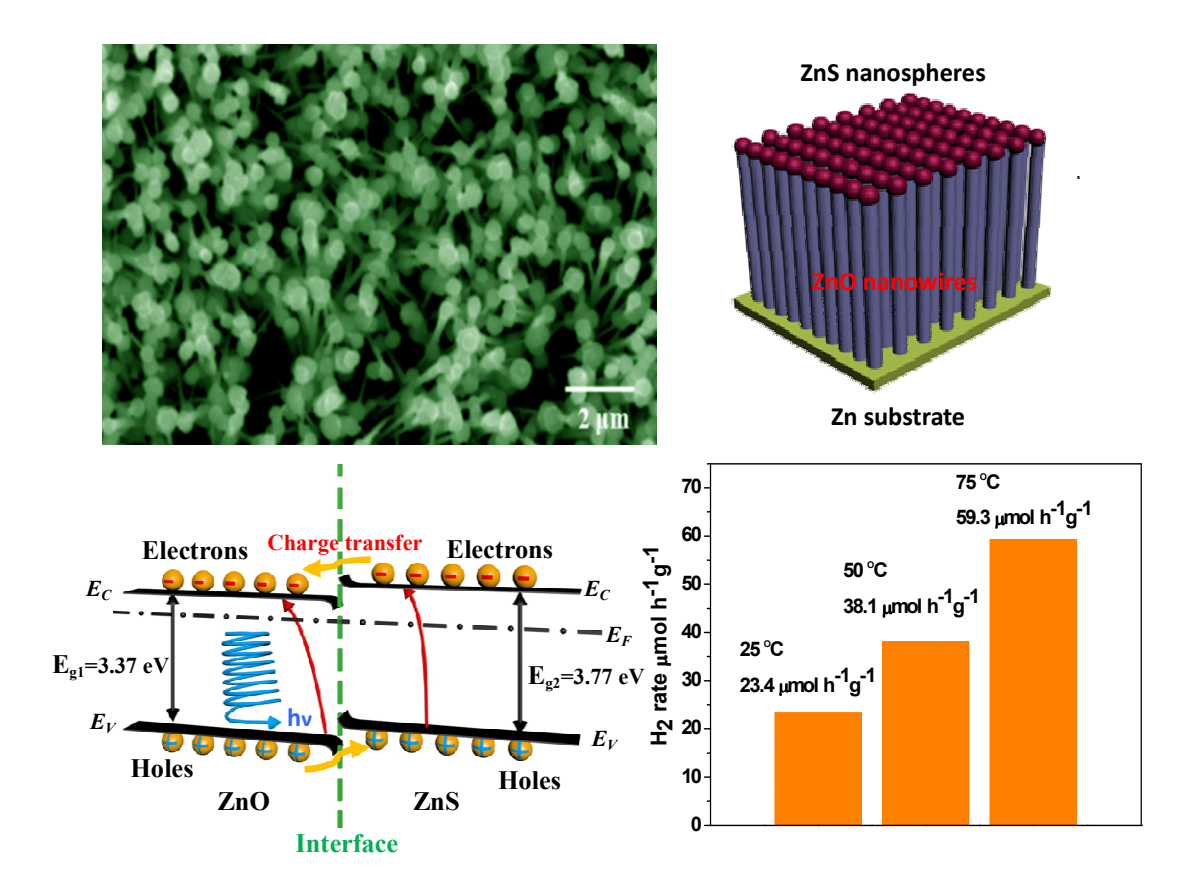
Accepted Manuscripts are published online shortly after acceptance, before technical editing, formatting and proof reading. Using this free service, authors can make their results available to the community, in citable form, before we publish the edited article. We will replace this Accepted Manuscript with the edited and formatted Advance Article as soon as it is available.

You can find more information about *Accepted Manuscripts* in the **Information for Authors**.

Please note that technical editing may introduce minor changes to the text and/or graphics, which may alter content. The journal's standard <u>Terms & Conditions</u> and the <u>Ethical guidelines</u> still apply. In no event shall the Royal Society of Chemistry be held responsible for any errors or omissions in this *Accepted Manuscript* or any consequences arising from the use of any information it contains.



Graphical abstract



The graphical abstract exhibits the SEM images and schematic representation of ZnO-ZnS heterostructure NW arrays, schematic energy band diagram and rates of the photocatalytic H₂ at different temperature.

ROYAL SOCIETY OF CHEMISTRY

CrystEngComm

ARTICLE

Novel ZnO-ZnS Nanowire Arrays with Heterostructue and Enhanced Photocatalytic Properties

Received 00th January 20xx, Accepted 00th January 20xx

DOI: 10.1039/x0xx00000x

www.rsc.org/

Xingxing. Gao, ^a Jian Wang, ^b Jianglong. Yu^{a,c} and Hongbo. Xu^{a*}

Well aligned ZnO-ZnS heterojunction nanowire arrays have been synthesized via a novel wet-chemical route in which ammonium persulfate was used as oxidant to oxidize zinc foil directly followed by a sulfidization process to substitution oxygen with sulfur in the alkali solution. The structure and photocatalytic properties of the ZnO-ZnS were analysed in comparison with that of ZnO nanowires. The formation mechanism of ZnO-ZnS heterojunction NW arrays arises from a combination of two different processes, namely a typical dissolution-crystallization process and a substitution reaction. Room temperature photoluminescence measurements indicate that ZnO-ZnS heterojunction NW arrays have an emission peak cantered at 385 nm, and the PL intensity of ZnO-ZnS heterojunction is lower than that of ZnO NW arrays. The morphology and structure of the heterostructural products have been characterized by transmission electron microscopy (TEM), energy dispersive spectroscopy (EDS), and X-ray photoelectron spectroscopy (XPS). Due to the formation of heterostructures and a new transfer pathway of electrons from ZnS to ZnO, the composites show significantly improved photocatalytic activities than that of pure ZnO NW arrays. This study persuades a novel way of fabricating semiconductor composites for high-efficiency photocatalysis applications.

Introduction

One-dimensional (1D) semiconducting nanostructures have attracted extraordinary attention in the past few decades due to their unique properties and superior performances.¹⁻³ Recently, 1D nano/heterostructures consisting of two important functional materials are attracting increasing interests because of the possibility of tuning their chemical, electronic, and optical properties over a wider range and performing diverse functionalities within a single nanostructure. 4-6 Motivated by these prospects, significant progress has been made in the synthesis of various 1D heterostructured nanostructures including Si-SiGe and GaAs-GaP superlattice nanowires, biaxial TiO₂-SnO₂, ZnO-Ge, CdSe-Si, and ZnS-Si nanoribbons, which provide a testing ground to study the fundamental effects of different components and their interface on the optical and electronic properties of nano-heterostructures.7-15 Among the various semiconductor heterostructure nanostructures, ZnO-ZnS nano-heterostructures are considered as the most promising materials due to their excellent optical and electrochemical properties. 16-18 As an important II-VI semiconductors, zinc oxide (ZnO) has a wide band gap energy

On the other hand, ZnS has a wide band gap energy of 3.66 eV at room temperature.²⁸ It is a well-known luminescent material, having prominent applications in flat-panel displays, electroluminescent devices, sensors, and lasers, and also has been applied in photocatalysts, infrared windows, pigmen s, and nonlinear optical devices.^{29,30} ZnO-ZnS heterostructures have become of prime importance because of the lower photoexcitation threshold energy and improved electron transfer paths.^{31,32} Both theoretical calculations and experimental results have demonstrated that ZnO-ZnS heterostructures exhibited higher photocatalytic efficiencies for the degradation of several dye pollutants in both acidic and

of 3.37 eV with a large binding energy (E_B=60 meV). 19-21 It is an excellent candidate for photocatalysts, photodetectors, and ultraviolet laser. 22-24 However, it can absorb only UV light with the wavelength equal to or less than 385 nm and greatly limits its practical application in environmental decontamination.²⁵ Furthermore, the photocatalytic action of a semiconduct particulate system is based on generation of electron-hole pairs. In order to obtain high reaction efficiency, the recombination of the two kinds of charge carriers must be kept low. 26,27 Thus, how to extend energy range of photoexcitation and enhance photocatalytic activity of ZnO has become a challenge work on solar energy conversion and environmental cleaning. In order to enhance the photocatalytic performance of ZnO photocatalysts, coupling/doping of ZnO with other semiconductors (with wide or narrow band gaps) can facilitate the separation of photogenerated hole-electron pairs and regulate band-gar energies, which has been studied widely as an efficie t approach.

^{a.}School of chemical Engineering, University of Science and Technology Liaoning, High-Tech District 185 Qianshan Middle Road, Anshan 114051, China

^b School of mining Engineering, University of Science and Technology Liaoning, High-Tech District 185 Qianshan Middle Road, Anshan 114051, China ^cChemical Engineering, University of Newcastle, Callaghan NSW2308, Australia

E-mail: Inkdxhb@163.com; Fax: +86 4125928573; Tel: +86 4125928573 Electronic Supplementary Information (ESI) available: [SEM images pure ZnO NW arrays and ZnO nanorod arrays]. See DOI: 10.1039/x0xx00000x

ARTICLE CrystEngComm

basic medium than the individual components due to their type-II band alignments. 33,34 For instance, ZnO core/ZnS shell structures have been successfully synthesized by Chen et al., which showed excellent photocatalytic properties.³⁵ Hu and coworkers have prepared ZnO/ZnS core-shell nanorods which possess significantly higher visible light photocatalytic activity.36 Besides, Lu have reported that vertically aligned ZnO-ZnS heterojunction nanowire (NW) arrays which were used for converting mechanical energy into electricity, were synthesized by a thermal evaporation method.³⁷ However, the facile and simple synthesis of ZnO-ZnS heterostructure NW arrays remains a challenge until date. This is mainly due to the high sensitivity of such heterostructures to synthetic conditions, such as, oxidation propensity of ZnS surfaces as well as differential solubility of the constituents in the catalyst particle. Therefore, for the more effective synthesis of hybrid or ZnO-ZnS heterostructures, there is an urgent need to develop a new and promising method that is simple, convenient and free of contamination.

In this study, we report for the first time the epitaxial growth of ZnS nanospheres onto vertically aligned ZnO NW arrays to form ZnO-ZnS heterostructure NW arrays without any catalyst via a simple hydrothermal process. The formation mechanism of the ZnO-ZnS heterostructure NW arrays is suggested according to a series of experiments. The ZnO-ZnS heterostructure NW arrays integrate the optical properties of the components within them and exhibit different photoelectrochemical properties from ZnO NW arrays. Photocatalytic water splitting and photocatalytic degradation of an organic dye were performed in order to determine the performance of the catalytic synthesized ZnO-ZnS heterostructure NW arrays.

Results and discussion

XRD analysis

The crystal structure and crystal orientation of ZnO-ZnS heterostructure NW arrays are investigated by XRD diffraction. Fig. 1 shows the XRD pattern of the as-prepared ZnO-ZnS heterostructure NW arrays covered on the zinc foil substrate. The indexed diffraction peaks show a pure hexagonal phase of wurtzite-type ZnO (space group: P63mc) with lattice constants a = 3.249 Å and c = 5.206 Å, which is consistent with the database (JCPDF 80-0075). The highly enhanced (002) peak can be clearly seen as a result of the vertical orientation of ZnO NWs. On the same pattern, some weak peaks can be indexed as a typical face-centered ZnS (JCPDF 80-0020) and the hexagonal Zn phase (JCPDF, 04-0831) originating from the Zinc substrate. Because the diffraction peaks of (102) crystal plane of ZnO are very close to the peaks of (220) crystal plane of ZnS, two peaks are overlapped. It is worth noting that compared to the standard pattern of hexagonal phase ZnO the relative intensity of the peaks corresponding to (002) plane is significantly enhanced in the obtained XRD pattern (Fig. 1), which suggests that ZnO (001) plane is oriented parallel to the basal plane of the zinc foil substrate. Due to crystalline lattice mismatch between ZnO and ZnS, the atomic distance of Zn-O and Zn-S would be changed when the formation of ZnO-ZrS heterostructure NW arrays, which resulted in the distortion of crystal planes and shifts of XRD peaks. The selection of zinc foil as the substrate for the growth of well-orientated ZnO-ZnS heterostructure NW arrays is due to the following reason: the lattice matching between ZnO and Zn crystals (both are in the hexagonal phase) facilitates the growth of well-aligned ZnO-ZnS heterostructure NW arrays; moreover, zinc foil is a conductive material, making it easy to utilize the aligned ZnOheterostructure NW arrays for electronic optoelectronic devices.

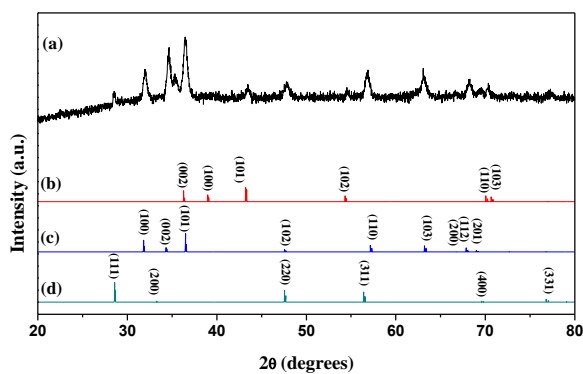


Fig. 1 (a) XRD pattern of well-aligned ZnO-ZnS NW arrays on the Zinc foil substrate; (b-d) standard diffraction patterns of Zn (4-0831), ZnO (80-0075) and ZnS (80-0020) shown as references.

Surface morphology

Fig. 2 shows the large arrays of oriented ZnO-ZnS heterostructure NWs, which are vertically grown on a zinc fon substrate along the [001] direction. The top view (Fig. 2a and b) shows that ZnO-ZnS heterostructure NWs cover the zinc surface uniformly. The images at higher magnifications (Fig. 2c and d) clearly shows that ZnO NWs are aligned well on to the zinc substrate with the average diameter of about 100 nm and every tip of the ZnS multipods has been capped by a nanosphere with the average size around 400 nm. It is interesting that the ZnS nanospheres were not found at the other area.

Structural and composition analysis

Further observation under HRTEM found that the nanospheres on the tips of ZnO-ZnS heterostructure NW arrays were essentially agglomerates of many small crystallite grains, as shown in Fig. 3. It can be seen that ZnS nanospheres grow on the tip of ZnO NWs and ZnS nanospheres consist of much smaller (~25 nm), nanocrystals (Fig. 3a), compared to the roughly spherical 300 nm particles agglomerate as shown in Fig. 2a. This is consistent with the results of SEM analysis. An HRTEM image shown in Fig. 3b is taken from the interfacial region (circular area marked 'b' in Fig. 3a) between the ZnO-rod and ZnS-grain side. It can be seen that the interfacial region is clean and uniform at the atomic scale. Lattice fringers spacing of 0.260 nm and 0.299 nm were measured

ARTICLE CrystEngComm

Fig. 2 SEM images of the ZnO-ZnS heterostructure NW arrays grown directly on Zn substrate: (a) and (b) low-magnification tilt view; (c) and (d) high-magnification images of ZnO-ZnS heterostructure arrays.

corresponding to that of the (002) and (111) lattice plane of the wurtzite ZnO (JCPDF 80-0075) and sphalerite ZnS (JCPDF 80-0020), respectively. An epitaxial growth of ZnS above ZnO NW was observed at the interface. It can also be seen that a thin intermediate layer is found in between, which is due to the large lattice mismatch/dislocation between ZnO and ZnS. In order to reveal the chemical compositions of the granular particle and nanowire, the area marked by box I and box II in Fig. 3a were analyzed with EDS spectroscopy. From the corresponding EDS spectra (insets in Fig. 3c and d), it can be seen that the elements in the isometric particle are Zn and S and the elements in the NWs are Zn and O (the signals of C and Cu in the EDS spectra originate from the carbon-coated copper grid onto which the sample was deposited). EDS analysis of the other areas of the NWs reveals that the elements were consistently Zn and O. These results suggest that the granular particles are ZnS grains while the NWs are pure ZnO. EDS analysis of the other area of the branch reveals that the elements are still Zn and O. These results suggest that the granular particle is composed of ZnS while the NW is still pure ZnO. SAED patterns (Fig. 3c and d) taken on the same sites as those in EDS analysis also provide important information about the structures of the granular particle and the NWs. The indexing of the SAED patterns demonstrates that the granular particle is polycrystalline ZnS with a face-center cubic structure and the NW is wellcrystalline ZnO with a hexagonal structure, which is consistent with XRD and EDS studies. To elucidate the formation of the ZnS nanospheres on the tip of ZnO NWs, XPS analysis was

carried out. Fig. 4a is the XPS survey spectrum in which Zn, O, S and C peaks can be clearly be observed. The peaks at the binding energy 531.5 eV (Fig. 4b) are ascribed to the lattice oxygen in the ZnO-ZnS structure. 38 The O 1s photoelectron peaks are higher than the binding energy of O in ZnO, which is normally between 529.9 to 531.2 eV. The shoulder at a higher binding energy could be attributed to the presence of OH groups or adsorbed oxygen species or of oxygen atoms related to oxygen vacancies, possibly indicating different species between ZnO-ZnS heterostructure NW arrays and ZnO.³⁹ The spectrum in Fig. 4c shows the S2p 3/2 peaks located at 161.3 eV, are related to Zn-S bonding. These binding energy are smaller than those of sulfur and related compounds, such as S⁰, SO₂, SO₃²⁻, SO₄²⁻, which are typical for S²⁻ ions. 40 It indicat s that the existence of S element in the ZnO-ZnS structure. The binding energy of Zn2p_{3/2} and Zn2p_{1/2} peaks located at 1020.8 and 1043.2 eV are shown in Fig. 4d. The XPS spectra confirmed that ZnO on the surface of nanowire is sulfuretted and has been converted into ZnS, resulting in formation of ZnO-ZnS heterostructure NW arrays.

Growth Mechanism

The effects of reaction time and temperature on the growth of ZnO-ZnS heterostructure NW arrays were carefully investigated. The morphologies of pure ZnO NW arrays obtained at low hydrothermal temperature (at 120 °C) for 6 h and 12 h are shown in Fig. S1a and b, respectively. When the hydrothermal reaction was 6 h, ZnO NWs are aligned

ARTICLE CrystEngComm

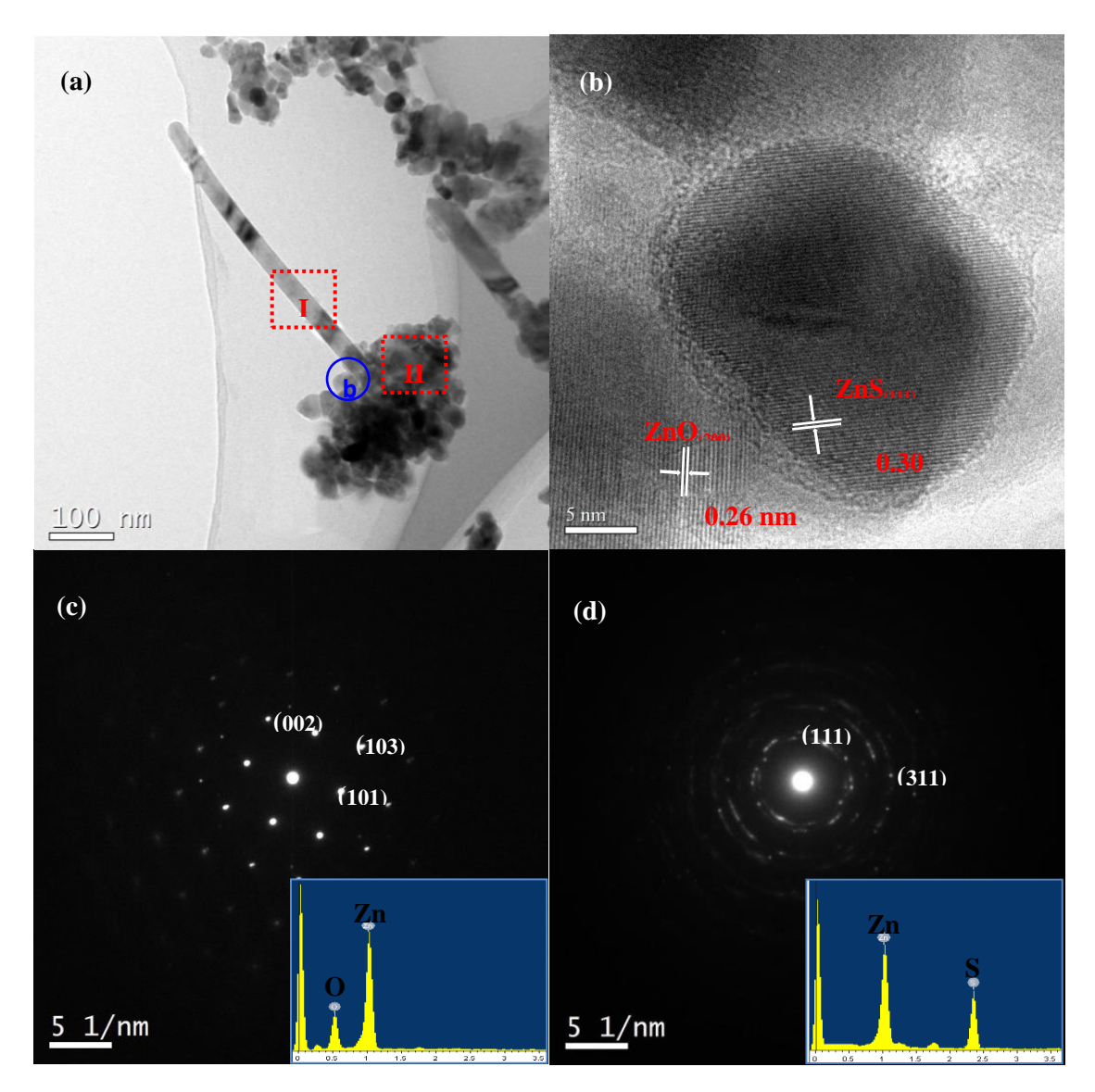


Fig. 3 TEM images of ZnO-ZnS heterostructure NW arrays: (a) TEM image of an individual NW capped by agglomerated particles; (b) HRTEM image of ZnO-ZnS heterostructure arrays interface of the two phases; (c) and (d) SAED patterns taken in the region marked by box I and II in (a), respectively. The inset of (c) and (d) show EDS spectra taken from the region marked by box I and II in (a), respectively, indicating ZnS nanospheres and ZnO nanorods.

approximately normal to the zinc substrate with a diameter of about 50-100 nm. As the reaction time increased to 12 h, the length of ZnO NW arrays became longer, while the diameter did not change significantly. During the hydrothermal growth process, the temperature of the hydrothermal system is the critical parameter for the formation of ZnO-ZnS heterostructure NW arrays. Only pure ZnO nanorod arrays were obtained when the hydrothermal treatment was increased to 160 $^{\circ}$ C for 12 h (Fig. S1c). As shown in Fig. S1c, the length of these ZnO nanorod arrays with an average diameter of 300 nm and the NWs became much longer than ZnO NW arrays. This indicates that the formation of ZnS nanospheres needs a high-temperature condition (220 $^{\circ}$ C) rather than a low-temperature condition (160 $^{\circ}$ C). In the current reaction process, as the initial hydrothermal temperature is low (120 $^{\circ}$ C), SCN did not

decompose to release S^2 , therefore no ZnS nanospheres we cobserved. In contrast to ZnO NW arrays and ZnO nanorc arrays, the diameter of ZnO-ZnS heterostructure NW arrays is smallest. It demonstrates that ZnS formed from S^2 that is released from S^2 upon a high-temperature (220 $^{\circ}$ C) hydrolyzation process reacted with ZnO NW arrays, leading to the reduction in diameter of ZnO-ZnS heterostructure N°V arrays.

Based on the above observations and analyses, a combination of two different processes, namely a typical dissolution-crystallization process and a substitution reaction are believed to be responsible for the growth of well-aligned ZnO-ZnS heterostructure NW arrays. The mechanistic conversion process from ZnO NW arrays to ZnO-ZnS heterostructure NW arrays is schematically shown in Fig. 5. The Zn foil serves as both a

CrystEngComm ARTICLE

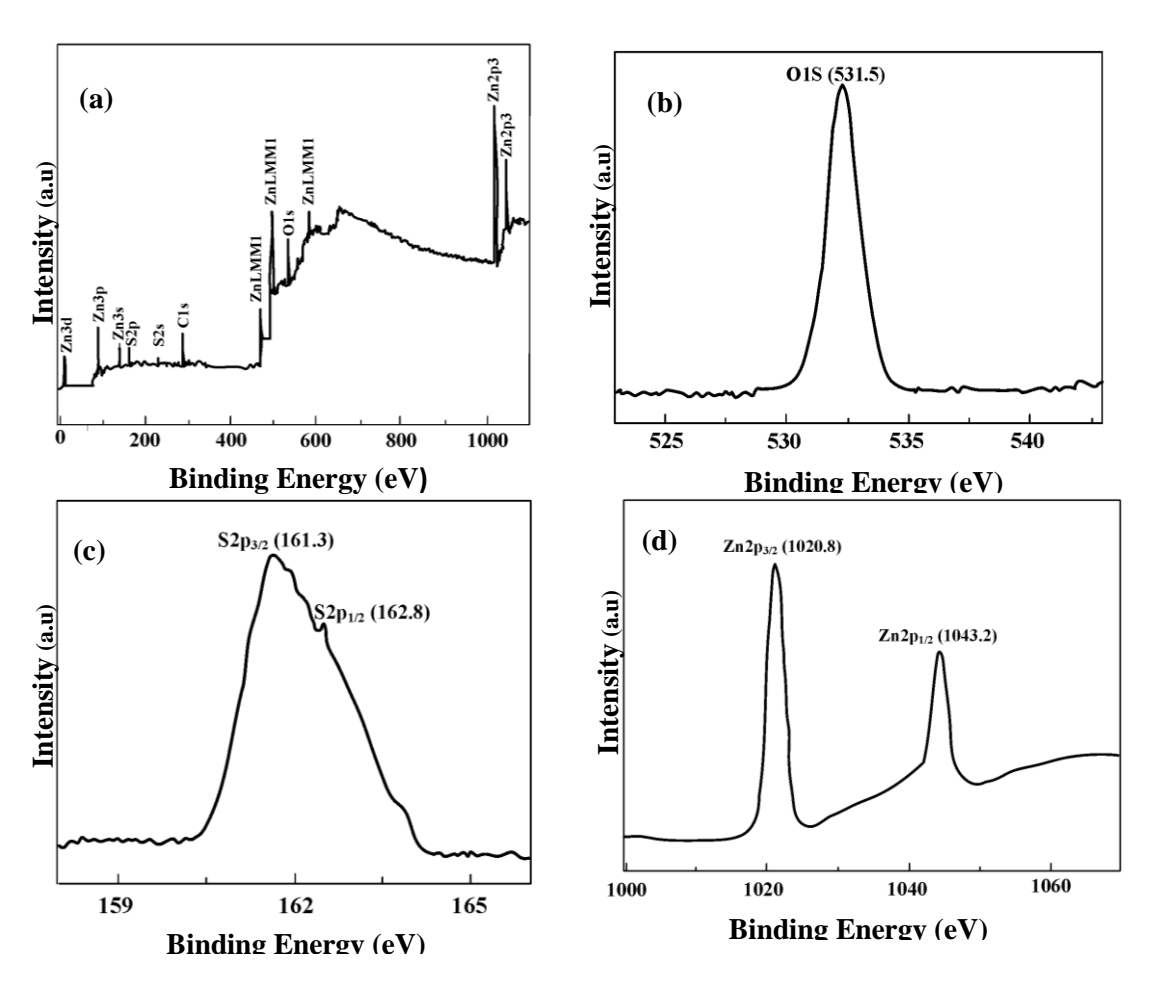


Fig. 4 XPS spectra of ZnO-ZnS heterostructure NW arrays: (a) complete survey and O1s, (c) S2p, and (d) Zn2p peaks.

substrate and the zinc source. At the beginning of the low temperature hydrothermal reaction (120 °C), the zinc surfaces are first oxidized by (NH₄)₂S₂O₈ into a large quantity of ZnO thin films, which serve as the nuclei and reduce the interface energy barrier for the crystal growth. At the same time, the fresh resulting ZnO thin films can be dissolved in the KOH solution as [Zn(OH)₄]⁻² growth units into the solution. More growth units of [Zn(OH)₄]⁻² can be successively supplied with the oxidation of zinc foil by (NH₄)₂S₂O₈. Consequently, the resulting [Zn(OH)₄]⁻² could serve as growth units for the epitaxial growth of nuclei into 1D ZnO structures as soon as they reach a critical saturation point. With respect to the structure of ZnO, the polar growth of ZnO crystal along the [001] direction proceeds through the adsorption of growth units of $[Zn(OH)_4]^{2-}$ onto the (001) plane and the side surfaces are {01-1} and/or {2-1-1} due to their lower energies than that of (001) [40]. These nuclei would preferentially grow along the [001] direction to form 1D nanowires if the chemical environment constantly provides [Zn(OH)₄]²⁻ growth units, which can be realized in our reaction system. 41 As the reaction continues at low temperature (120 °C), ZnO NW arrays will keep on growing. The introducing of KSCN in the current hydrothermal system is vital for the formation of ZnO-ZnS heterostructure NW arrays. In the next high-temperature hydrothermal reaction, ZnO NW arrays are used as a selftemplate for the fabrication of ZnO-ZnS heterostructure NW arrays with an increase in OH concentration. The ZnS nanospheres forms in the sulfidation process of ZnO NW precursor crystals at 220 °C, in which S²⁻ that is released from SCN upon a high-temperature hydrolyzation process serves as sulfur source. After that, S²⁻ readily reacts with ZnO at the surface of the ZnO NW arrays to produce ZnS nucleates and grows on the tip of ZnO NW arrays due to their higher surface energy compared with other areas such as the side of NWs, but in contrast, the diameter of ZnO NW arrays decreases. The high-temperature hydrothermal reaction can improve to nucleation rate of ZnS nuclei and then, ZnS nuclei would growlarger and larger to form ZnS nanospheres along with the process of reaction, which bring about the formation of ZnO-ZnS heterostructure NW arrays.

Optical Property

To check for the absorbance of the photocatalysts, the diffuereflection spectra (DRS) are discussed. Fig. 6a shows the DRS of ZnO NW arrays and ZnO-ZnS heterostructure NW arrays, which reveal the remarkable change of the optical absorption property. For bare ZnO NW arrays, only a UV absorption band is observed. The absorption edge of ZnO NW arrays locates at 370 nm close to the value for bulk ZnO ($E_g = 3.37$ eV). The ZnO NW arrays show no absorption in the visible region. A

ARTICLE

ZnS heterostructure
m of the ZnO NW
structure NW arrays
which indicates the
the photogenerated
e tip of ZnO NW
materials were also
separation of the
thus, the ZnO-ZnS
gher photocatalytic

NW arrays

nO-ZnS
ostructure
/ arrays

significant red shift in the absorption edge is observed in the UV-vis DRS spectrum of the ZnO-ZnS heterostructure NW arrays because of deposition of ZnS nanospheres on the tip of ZnO NW arrays and the photo absorption in the visible region at the range of 375-650 nm was obviously enhanced. This red shift is attributed to the electronic interaction between ZnO and ZnS upon the increase of ZnS on the tip of ZnO NW arrays.⁴³ Furthermore, the ZnS nanospheres grown after the formation of ZnO NW arrays lead to a coarser surface, which diminishes the reflection of incident light, and then increases the volume of the optically active component.⁴⁴ These results indicate that the shape of ZnO nanowires and both the interface between the ZnS nanospheres and ZnO NW arrays play significant roles in the photo absorption of ZnO-ZnS heterostructure NW arrays. Therefore, the absorption ability of the ZnO NW arrays can be tuned by using such simple sulfidation process.

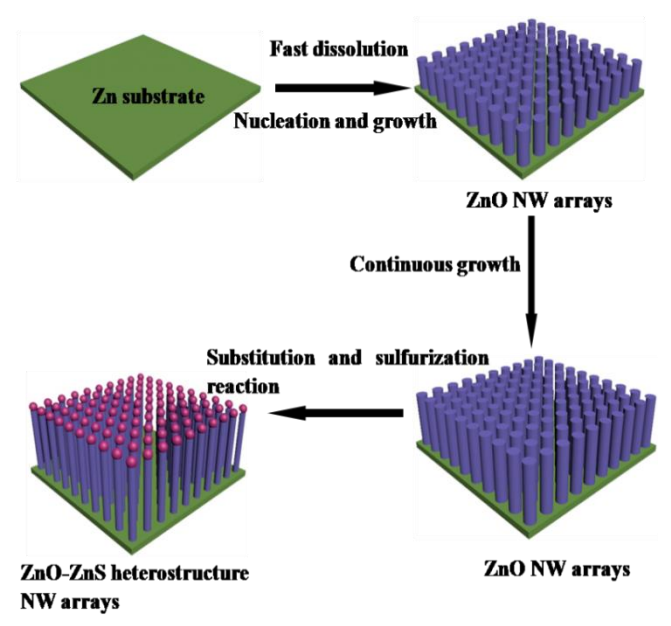
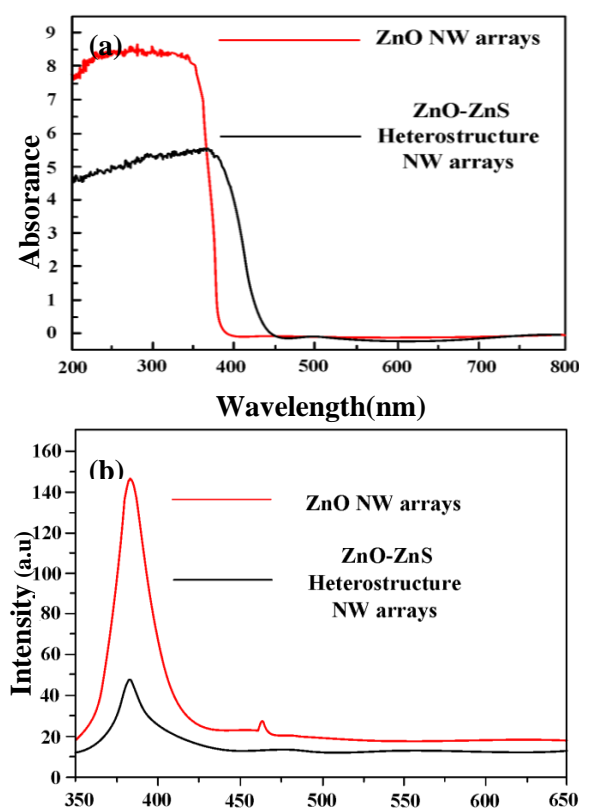


Fig. 5 Schematic representation of the fabrication of well-aligned ZnO-ZnS heterostructure NW arrays on the zinc foil from a facile ZnO self-template.

Photoluminescence (PL) was performed at room temperature and Fig. 6b compares the results of the PL measurements of the ZnO-ZnS heterostructure NW arrays and ZnO NW arrays. The PL spectrum of the ZnO NW arrays, in which an ultraviolet emission with peak at 385 nm and a weak blue band centred at 470 nm, can be observed. The ultraviolet emission was reported to be due to oxygen interstitials, 45 suggesting oxygen excessive in the ZnO NWs. The origin of the blue emission could be attributed to the defect related emission. 46.47 Interestingly, no significant emission in the green region could be detected that corresponds to a transition from a single ionized oxygen vacancy in the ZnO NWs.48 It is known that, in the case of solution phase synthesis, the relative concentration of OH⁻/Zn²⁺ regulates the luminescence properties of ZnO crystals and that the green intensity decrease was at a minimum. Furthermore, ZnO-ZnS heterostructure NW arrays did not show the blue and green luminescence. During the next hydrothermal process at 220 °C, sulfur anions could diffuse into the surface oxygen

vacancies in ZnO that can act as active trap sites for electrons and occupy their sites. Thus, the blue emission and green emission could almost disappear in ZnO-ZnS heterostructure NW arrays. Compared to the PL spectrum of the ZnO NW arrays, the PL intensity of ZnO-ZnS heterostructure NW arrays is reduced, especially in UV region, which indicates the suppression of the recombination of the photogenerated electron-hole pair by ZnS capped on the tip of ZnO NW arrays. ⁴⁹ The photocatalytic activities of the materials were also governed by the efficiency of the separation of the photogenerated electrons and holes. ⁵⁰ Thus, the ZnO-ZnS heterostructure NW arrays display higher photocatalytic activities than pure ZnO NW arrays.



Wavelength (nm)

Fig. 6 The corresponding UV-Vis DRS (a) and PL (b) of ZnO NW arrays and ZnO-ZnS heterostructure NW arrays.

Photocatalytic Property

The photocatalytic proterties of the ZnO-ZnS heterostructure NW arrays and ZnO NW arrays were investigated, taking the degradation of MO under UV-light irradiation ($\lambda > 324$ nm). Fig. 7a shows the photocatalytic degradation activity of meth 'l orange (MO) solution using different photocatalysts under the same conditions and the characteristic absorption of methy' orange (MO) approximately 464 nm was used to monitor the process of degradation, where C_0 and C are the initial concentrations of methyl orange (MO) after the equilibrium adsorption and that after the reaction, respectively. The addition of catalysts significantly accelerates the decomposition process, and the degradation rate also exhibits a remarkable dependence.

CrystEngComm ARTICLE

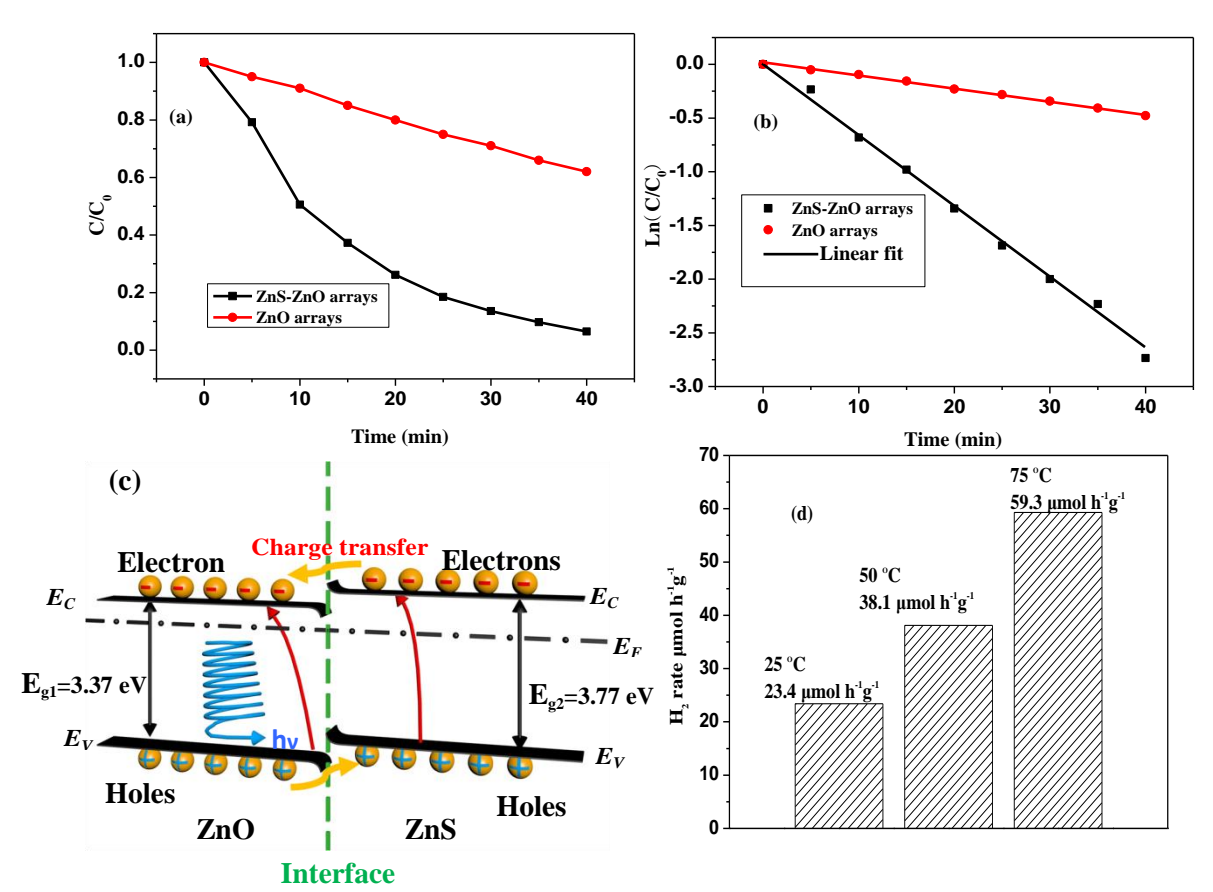


Fig. 7 (a) Comparison of the photocatalytic activity of ZnO nanowire arrays and that of ZnO-ZnS heterostructure arrays. (b) The linear fitting of the photocatalytic activity. (c) Schematic energy band diagram for ZnO-ZnS heterostructure arrays after UV irradiation. (d) Rates of the photocatalytic H_2 at different temperature (Light source: Hg-arc (300 W) with UV cut-off filter $\lambda > 420$ nm).

on the heterostructures. For pure ZnO NW arrays, the degradation rate in only 62% after 40 min under UV-light irradiation. As seen in Fig. 7a, with ZnO-ZnS heterostructure arrays as photocatalysts, MO was nearly completely degraded by UV-light irradiation after 40 min, which is evidently higher than for the above-mentioned pure ZnO NW arrays. The photocatalytic dye decomposition follows the Langmuir-Hinshelwood kinetic model.⁵¹ For this model, which can be given as $In(C/C_0) = k_{app}t$, the first-order linear relationship is extracted from the plots of In(C/C₀) versus irradiation time (t), where C_0 is the initial concentration of the MO dye, C is the concentration of the MO dye at different UV illumination times, k_{app} is the apparent first-order reaction constant, and t the irradiation time. Fig. 7b shows degradation of methyl orange (MO) with the presence of catalysts which follows a pseudofirst-order kinetic formula. The average value of apparent rate constant for ZnO-ZnS heterostructure NW arrays (k = 0.072 min^{-1}) is 5.1 times higher than ZnO NW arrays (k = 0.014 min⁻¹) 1). In contrast, when the ZnO-ZnS heterostructure NW arrays were used as photocatalysts in the system, significant enhancement effect of the photocatalysis was observed. Methyl orange (MO) was decomposed thoroughly within 40 min giving the highest value of 0.081 min⁻¹, which is more than 5.8 times higher than ZnO NW arrays. It is well known that the charge separation and transport are crucial for high-efficiency

photocatalysts. In order to reveal the reason for the superior photocatalytic activity of ZnO-ZnS heterostructure NW arrays, the energy band structures of ZnO and ZnS are schematically illustrated in Fig. 7c. The conduction band of ZnS lies at a more negative potential than that of ZnO, while the valence band of ZnO is more positive than that of ZnS.⁵² In this case, following the generation of electron-hole pairs under UV illumination, the electrons will move to the ZnO side and holes will move to the ZnS side due to the internal field at the ZnS-ZnO interface. facilitating the formation of a charge transfer state and the spatial separation of the photo-generated carriers within the ZnO-ZnS arrays.⁵³ The spatial separation of the photogenerate carriers can decrease the recombination of the electron-hole pairs. Based on the analysis of PL results, the photogenerated electrons and holes separated at the ZnO-ZnS interfaces could increase both the yield and the lifetime of charge carriers, which restrains their recombination probability and enabl s them to migrate effectively to the surfaces of ZnO and Zn respectively, resulting in the formation of the hydroxyl radical species ('OH).54 As a powerful oxidant, the hydroxyl radical could decompose MO effectively, and thus the photocatalytic efficiency may increase significantly. The stability and reusability of ZnO-ZnS heterostructure NW arrays was shown in Fig. S2.

ARTICLE CrystEngComm

The ZnO-ZnS heterostructure NW arrays were used as the photocatalyst for photocatalytic H₂ production under visible light (λ > 420 nm) irradiation. Fig. 7d shows that ZnO-ZnS heterostructure NW arrays exhibit active visible-light-driven H₂ evolution with a rate of 23.4 $\mu mol~h^{\text{--}1}g^{\text{--}1}$ at 25 $^{\circ}\text{C}$. In contrast, no H₂ evolution was observed for commercial ZnS, ZnO samples and ZnO NW arrays due to their large band gap.⁵⁵ It is well known that both ZnS and ZnO have a large band gap, and thus almost no absorption in the visible light region. The effect of reaction temperature on photocatalytic water splitting performance has been investigated in the range of 25-75 °C (Fig. 7d). An increase in temperature significantly enhances the rate of hydrogen evolution. The increased reaction rate can be attributed to the effect of temperature on "dark" reaction steps, such as the adsorption-desorption equilibrium of reactants and products and the diffusion of adsorbed species.⁵⁶ A schematic for H₂ splitting scheme was shown in Fig. S3.

In the ZnS-ZnO heterostructure arrays, the ZnS nanospheres were capped on the tip of the ZnO NWS. This created numerous ZnS-surface-states on ZnO NW surfaces. The electrons at the ZnS-ZnO interfaces could be excited from the bent VB level induced by the ZnS surface states to the CB of ZnO for water reduction. In this way, the effective band gap at the interface would be narrowed, which enables excitation under visible-light irradiation. The photogenerated holes would be trapped by the ZnS-surface-states and subjected to quenching by the sacrificial reagent (S²/SO₃²-) that facilitates the electron-hole separation. These results indicate that compared with ZnO NW arrays, the ZnS-ZnO heterostructure arrays improve the separation efficiency of the photo-generated intermediates and reduce the energy barrier at the interface. Therefore the ZnO-ZnS NW arrays show remarkably improved photocatalytic performance.

Conclusions

Well-aligned ZnO-ZnS heterostructure NW arrays were successfully grown on zinc foil substrates through direct oxidation of zinc foil using ammonium persulfate as oxidant followed by a sulfidization process to substitute oxygen with sulfur. ZnS nanospheres with a size 200 nm were grown on the tip of ZnO nanowires. Compared to ZnO NW arrays, the PL spectra of ZnO-ZnS heterostructure NW arrays at room temperature showed a decreased UV emission, showing the suppression of the recombination of the photogenerated electron-hole pair. ZnO-ZnS heterojunction arrays exhibited a significantly higher photocatalytic activity for the degradation of methyl orange (MO) than that of ZnO NW arrays under the same conditions. ZnO-ZnS heterostructure arrays also exhibited a higher photocatalytic performance for H₂ evolution from water splitting. The ZnO-ZnS heterostructure NW arrays have a H₂ production of 23.4 μmolh⁻¹g¹ under visible light irradiation at 25 °C. ZnO-ZnS heterostructure NW arrays could create ZnSsurface-states on the ZnO nanowire surfaces, which induce band bending of ZnO and narrow down the effective band gap at the interface of the ZnO-ZnS hybrids, thus allowing visiblelight excitation. The enhanced photocatalytic performance is attributed to the improved electric conductivity of ZnO-ZnS heterostructure NW arrays and increased the light utilization through broadening the light absorption range.

Experimental section

Synthesis of ZnO-ZnS heterostructure NW arrays. All chemical reagents were of analytical grade and were used as received without further purification. Zinc foil (99.99%, Aldrich) was ultrasonically washed in absolute ethanol before use. For the synthesis, the starting solution was prepared by mixing 15 mL of 3.2 mol/L KOH solution and 15 mL of 0.24 mol/L ammonium persulfate solution under stirring. Then 2-4 mmol KSCN were added under stirring. The mixture was then transferred into a 50 mL Teflon-lined autoclave, followed by immersing a piece of zinc foil ($2\times2\times0.8$ cm) in the reactare solution. The autoclave was sealed and maintained at 120 °C for 12 h, and was then heated at 220 °C for 12 h. Aftareaction, the solution was cooled down to room temperature. The zinc foil was then taken out of the solution, washed with absolute ethanol, and finally air-dried for further analysis.

Synthesis of ZnO NW arrays. The synthesis process of Zno NW arrays followed a similar procedure to that given above. The starting solution was prepared by mixing 15 mL of 3.2 mol/L KOH solution and 15 mL of 0.24 mol/L ammonium persulfate solution under stirring. Afterward, the mixture was transferred into a 50 mL Teflon-lined autoclave, followed by immersing a piece of zinc foil (2×2×0.8 cm) in the reactant solution. The autoclave was sealed and maintained at 120 °C for 6 and 12 h, respectively. After the solution was cooled to room temperature, the zinc foil was taken out of the solutio washed with ethanol, and finally air-dried for characterization. The ZnO nanorod arrays obtained with the next hydrothermal high temperature 160°C for 12 h and other reaction conditions similar to ZnO-ZnS heterostructure NW arrays.

Characterization. The as-synthesized samples were examined by X-ray diffractometry (XRD) (Rigaku-DMax 2400) equipped with graphite monochromatized $CuK\alpha$ ($\lambda = 1.5406$ Å). The morphology of the samples was investigated by using a scanning electron microscope (Hitachi S-3500N). The transmission electron microscopy (TEM) and high resolution microscopy (HRTEM) (Phisli s transmission electron CM200/FEG) were used to study the microstructure of the samples using an accelerating voltage of 200 kV. The photoluminescence spectrum was measured at room temperature in a spectral range of 350-600 nm using a Xe lamp with a wavelength of 325 nm as the excitation source. The formation of ZnS nanospheres on the tip of ZnO nanowires at 1 the bonding characteristics were determined by X-ray photoelectron spectroscopy (XPS, ESCALAB 250). UV-V. diffuse reflectance spectroscopy (DRS) and absorption spectra of various samples were measured using a Hitachi U-3010 spectrophotometer at room temperature.

Photocatalytic degradation of organic dye. The photocatalytic activities of ZnO-ZnS heterostructure NW arrays

CrystEngComm ARTICLE

as photocatalysts were compared against ZnO NW arrays by measuring the photodegradation of methyl orange (MO). Zn substrate with ZnO-ZnS heterostructure NW arrays (2×2×0.8 cm) was averagely separated into 10 pieces. Five pieces of a little Zn substrate with ZnO-ZnS heterostructure NW arrays were put in 15 mL of 10 ppm aqueous solution of MO. The mixture was stirred in the dark for 1 h to achieve the equilibrium adsorption. Then the suspension was exposed to UV light (300 W high pressure Hg lamp) for different durations. The concentration change of MO was monitored by measuring the UV-vis absorption of the suspensions at regular intervals. The suspension was centrifuged at 14000 rpm for 1 min to remove the photocatalysts before measurements. The peak absorbance of MO at 466 nm was used to determine its concentration.

Photocatalytic water splitting. Five pieces of a little Zn substrate with ZnO-ZnS heterostructure NW arrays were dispersed in an aqueous solution (20 mL) of Na₂S (0.25 M) and Na₂SO₃ (0.35 M). The suspension was sealed in a quartz flask and purged with argon for 1 h to flush out the residual air. The photocatalytic hydrogen production was initiated by irradiating the suspension with an Hg-arc lamp (350 W) coupled with a UV cut-off filter ($\lambda > 420$ nm) cooled with a fan. The concentration of H₂ was analyzed by a gas chromatography equipped with a thermal conductivity detector (molecular sieve 5-Å column and Ar as the carrier gas).

Acknowledgements

The authors gratefully acknowledge the financial support of Special Foundation of University of Science and Technology Liaoning (2011ZX14), Foundation of Anshan Municipal Division of Science & Technology (2013MS27), the Scientific Research Foundation of Department of Education of Liaoning Province (11202177).

References

- J. Liu, K. P. Song, P. A. Aken, J. Maier, Y. Yu, Nano Lett., 2014, 14, 2597.
- J. Wang, J. Liu, H. B. Xu, Z. S. Ma, S. M. Ji, Y. C. Zhou, P. Hodgson, Y. C. Li, J. Mater. Chem. A, 2013, 1, 1117.
- 3 J. Liu, Y. L. Wan, W. Liu, Z. S. Ma, S. M. Ji, J. B. Wang, Y. C. Zhou, P. Hodgson, Y. C. Li, J. Mater. Chem. A, 2013, 1, 1969.
- 4 M. Bierman, S. Jin, Energy Environ. Sci., 2009, 2,1050.
- 5 G. Z. Shen, D. Chen, C. W. Zhou, Chem. Mater., 2008, 20, 3788.
- Z. Jiang, Q. Qing, P. Xie, R. X. Gao, C. M. Lieber, *Nano Lett.*, 2012, 12, 1711.
- 7 Y. Wu, R. Fan, P. Yang, Nano Lett., 2002, 2, 83.
- M. S. Gudiksen, L. J. Lauhon, J. Wang, D. C. Lieber, *Nature*, 2002, 415, 617.
- 9 R. He, M. Law, R. Fan, F. Kim, P. Yang, Nano Lett., 2002, 2, 1109.
- L. W. Yin, M. S. Li, Y. Bando, D. Golberg, X. Yuan, T. Sekiguchi, *Adv. Funct. Mater.*, 2007, 17, 270.
- 11 X. H. Sun, T. K. Sham, R. A. Rosenberg, G. K. Shenoy, J. Phys. Chem. C, 2007, 111, 8475.
- 12 R. A. Rosenberg, G. K. Shenoy, X. H. Sun, T. K. Sham, Appl. Phys. Lett., 2006, 89, 243102.
- 13 J. Hu, Y. Bando, Z. Liu, T. Sekiguchi, D. Golberg, J. Zhan, J. Am. Chem. Soc., 2003, 125, 11306.

- 14 J. Yan, X. Fang, L. Zhang, Y. Bando, U. K. Gautam, B. Dierre, T. Sekiguchi, D. Golberg, *Nano Lett.*, 2008, 8, 2794.
- 15 C. W. Lin, D. Y.Wang, Y. Tai, Y. T. Jiang, M. C. Chen, C. C. Chen, J. Phys. D Appl. Phys., 2011, 44, 292002.
- 16 X. Fang, Y. Bando, U. K. Gautam, T. Zhai, H. Zeng, X. Xu, M. Liao, D. Golerg, Crit. Rev. Solid State Mater. Sci., 2009, 34, 190.
- 17 C. Lai, M. Lu, L. Chen, J. Mater. Chem., 2012, 22, 19.
- 18 J. S. Hu, L. L. Ren, Y. G. Guo, H. P. Liang, A. M. Cao, J. Wan, C. L. Bai, Angew. Chem. Int. Ed., 2005, 44, 1269.
- 19 X. S. Fang, Y. Bando, G. Z. Shen, C. H. Ye, U. K. Gautam, P. M. F. J. Costa, C. Y. Zhi, C. C. Tang, D. Golberg, *Adv. Mater.*, 2007, 19, 2593.
- 20 M. I. B. Utama, Q. Zhang, S. F. Jia, D. H. Li, J. B. Wang, Q. H. Xiong, ACS Nano, 2012, 6, 2281.
- 21 X. S. Fang, T. Y. Zhai, U. K. Gautam, L. Li, L. M. Wu, Y. Bando, D. Golberg, *Prog. Mater. Sci.*, 2011, 56, 175.
- 22 M. Chen, L. F. Hu, J. X. Xu, M. Y. Liao, L. M. Wu, X. S. Fang, Small, 2011, 7, 2449.
- 23 G. Murugadoss, V. Ramasamy, Spectrochimica Acta A, 2012, 93, 290.
- 24 J. L. Yang , S. J. An, W. I. Park, G. C. Yi, W. Choi, Adv. Mater., 2004, 16, 1661.
- 25 H. C. Ma, J. H. Han, Y. H. Fu, Y. Song, C. L. Yu, X. L. Dong, Appl. Catal. B: Environ., 2011, 102, 417.
- 26 M. A. Fox, M. T. Dulay, Chem. Rev., 1993, 93, 341.
- 27 M. I. Litter, Appl. Catal. B: Environ., 1999, 23, 89.
- 28 Z. Q. Wang, Z. Liu, J. F. Gong, S. Wang, S. G. Yang, CrystEngComm. 2011, 13, 6774.
- 29 X. Fu, X. Yang, Z. Qiu, F. Zhao, J. Zhuang, A. He, L. Chen, C. Wu, X. Duan, C. Liang, M. Wu, *CrystEngComm*, 2013, **15**, 3334.
- 30 J. Schrier, D. O. Demchenko, L. W. Wang, Nano Lett., 2007, 7, 2377.
- 31 J. Lahiri, M. Batzil, J. Phys. Chem. C, 2008, 112, 4304.
- 32 X. Fang, Y. Bando, U. K. Gautam, T. Zhai, S. Gradecak, D. Golberg, J. Mater. Chem., 2009, 19, 5683.
- 33 X. Yu, G. Zhang, H. Cao, X. An, Y. Wang, Z. Shu, X. L. An, F. Hua, New J. Chem., 2012, 36, 2593.
- 34 K. Zhang, D. W. Jing, Q. Y. Chen, L. J. Guo, Int. J. Hydrogen Energy, 2010, 35, 2048.
- 35 W. Chen, H. Ruan, Y. Hu, D. Z. Li, Z. X. Chen, J. J. Xian, J. Chen, X. Z. Fu, Y. Shao, Y. Zheng, J. J. Xian, J. Chen, X. Z. Fu, Y. Shao, Y. Zheng *CrystEngComm*, 2012, 14, 6295.
- 36 Y. Hu, H. H. Qian, Y. Liu, G. H. Du, F. M. Zhang, L. B. Wang, X. Hu, CrystEngComm, 2011, 13, 3438.
- 37 M. Y. Lu, J. Song, M. P. Lu, C. Y. Lee, L. J. Chen, Z. L. Wang, ACS Nano, 2009, 3, 357.
- 38 M. Ahmad, X. Yan, J. Zhu, J. Phys. Chem. C, 2011, 115. 1831.
- 39 E. Rauwel, A. Galeckas, P. Rauwel, M. F. Sunding, H. Fjellvag, J. Phys. Chem. C, 2011, 115, 25227.
- J. A. Rodriguez, T. Jirsak, S. Chaturvedi, M. Kuhn, Surf. Sci., 1999, 442.
 400.
- 41 C. Yan, D. Xue, J. Phys. Chem. B, 2006, 110, 25850.
- 42 L. Ye, W. Guo, Y. Yang, Y. Du, Y. Xie, Chem. Mater., 2007, 19, 6331.
- 43 Y. Zhang, Z. R. Tang, X. Fu, Y. J. Xu, ACS Nano, 2011, 5, 7426.
- 44 X. L Yu, J. G. Song, Y. S. Fu, Y. Xie, X. Song, J. Sun, X. W. Du, J. Phys. Chem. C, 2010, 114, 2380.
- A. B. Djurisic, Y. H. Leung, K. H. Tam, L. Ding, W. K. Ge, H. Y. Che S. Gwo, *Appl. Phys. Lett.*, 2006, 88, 103107.
- 46 W. D. Cheng, P. Wu, X. Q. Zou, T. Xiao, J. Appl. Phys., 2006, 100, 1.
- 47 J. P. Cheng, X. B. Zhang, X. Y. Tao, H. M. Hu, Z. Q. Luo, J. Phys Chem. B, 2006, 110, 10348.
- 48 J. X. Duan, X. T. Huang, E. K. Wang, H. H. AI, Nanotechnology, 2006, 17, 1786.
- 49 S. Balachandran, M. Swaminathan, Dalton Trans., 2013, 42, 5338.
- 50 Y. Wang, R. Shi, J. Lin, Y. Zhu, Energy Environ. Sci., 2011, 4, 2922.
- 51 C. Zhang, Y. F. Zhu, Chem. Mater., 2005, 17, 3537.
- 52 W. N. Jia, B. X. Jia, F. Y. Qu, X. Wu, Dalton Trans., 2013, 42, 14178.
- 53 S. S. Lo, T. Mirkovic, C. H. Chuang, C. Burda, G. D. Scholes, *Aav. Mater.*, 2011, 23, 180.
- 54 H. Gnaser, M. R. Savina, W. F. Calaway, C. E. Tripa, I. V. Veryovkin M. J. Pellin, Int. J. Mass Spectrom., 2005, 245, 61.
- 55 Z. Wang, S. W. Cao, S. Loo, C. Xue, CrystEngComm, 2013, 15 5688.
- 56 H. X. Sang, X. T. Wang, C. C. Fan, F. Wang, Int. J. Hydrogen Energ. 2012, 37, 1348.